

PMT: Plain Mask Transformer for Image and Video Segmentation with Frozen Vision Encoders

Niccolò Cavagnero Narges Norouzi Gijs Dubbelman Daan de Geus

Eindhoven University of Technology

Abstract

Vision Foundation Models (VFMs) pre-trained at scale enable a single frozen encoder to serve multiple downstream tasks simultaneously. Recent VFM-based encoder-only models for image and video segmentation, such as EoMT and VidEoMT, achieve competitive accuracy with remarkably low latency, yet they require finetuning the encoder, sacrificing the multi-task encoder sharing that makes VFMs practically attractive for large-scale deployment. To reconcile encoder-only simplicity and speed with frozen VFM features, we propose the Plain Mask Decoder (PMD), a fast Transformer-based segmentation decoder that operates on top of frozen VFM features. The resulting model, the Plain Mask Transformer (PMT), preserves the architectural simplicity and low latency of encoder-only designs while keeping the encoder representation unchanged and shareable. The design seamlessly applies to both image and video segmentation, inheriting the generality of the encoder-only framework. On standard image segmentation benchmarks, PMT matches the frozen-encoder state of the art while running up to $\sim 3\times$ faster. For video segmentation, it even performs on par with fully finetuned methods, while being up to $8\times$ faster than state-of-the-art frozen-encoder models. Code: <https://github.com/tue-mps/pmt>.

1. Introduction

Vision Foundation Models (VFMs), pre-trained at scale on large and diverse datasets, have established the Vision Transformer (ViT) [14] as the dominant encoder in modern computer vision. The DINO family [5, 39, 41] exemplifies this trend: by combining the ViT architecture with self-supervised objectives that promote dense and semantically rich representations, these models achieve strong performance in a broad range of downstream tasks without any task-specific design choices in the encoder itself.

The representational richness of VFMs enables a radical rethinking of downstream architectures. For instance, consider the task of image segmentation, which requires an

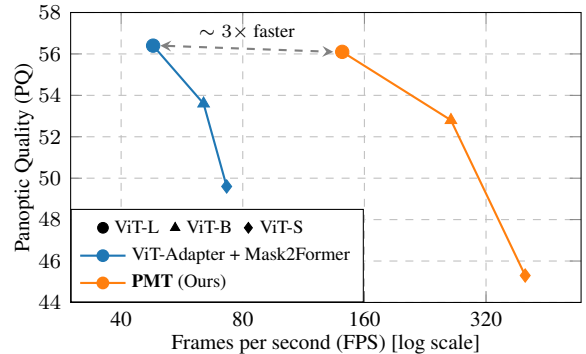


Figure 1. **ViT-Adapter + Mask2Former vs. PMT (Ours)**. PMT exhibits a better trade-off between Panoptic Quality and FPS across different sizes of frozen DINOv3 [41] pre-trained ViTs [14]. Evaluated on COCO val2017 [25], see Tab. 4.

image to be divided into pixel-level masks. Until recently, state-of-the-art ViT-based image segmentation models applied various task-specific components on top of the ViT, such as a convolutional adapter [9], a pixel decoder, and a Transformer decoder [10, 11, 19].

While this approach is effective, the Encoder-only Mask Transformer (EoMT) [20] method showed that these task-specific components are, in fact, largely unnecessary in combination with current VFMs. Specifically, EoMT consists of a plain ViT whose final layers are injected with a set of learnable queries, which are then processed alongside the patch tokens. During this process, each query accumulates the information needed to predict a binary segmentation mask and class label, allowing it to yield segmentation predictions with competitive accuracy at a fraction of the latency. The *encoder-only* framework was recently extended to the video domain, with VidEoMT [38]. Following the principles of EoMT, this model replaces task-specific tracking modules and temporal Transformer layers with a lightweight query propagation mechanism alongside the ViT, achieving 5–10 \times faster inference over prior art. Crucially, the success of this encoder-only paradigm requires sufficient scale, both in pre-training data and model size: without a sufficiently large and well-trained encoder, removing the specialized modules leads to a significant ac-

curacy drop [20, 38]. Only at scale does the pre-trained encoder alone carry the representational capacity previously distributed across many specialized modules, making those components largely redundant.

However, both EoMT and VidEoMT require *finetuning the entire encoder*. On the one hand, patch token representations must be updated to accommodate the segmentation task, requiring full finetuning of the encoder. More critically, because queries are injected into the self-attention layers, the pre-trained weights must adapt to incorporate these new tokens. As we empirically verify, freezing the encoder is not merely suboptimal, it fundamentally prevents the mechanism from working, as the pre-trained attention layers have no notion of the injected queries.

The fact that EoMT and VidEoMT require finetuning the ViT presents practical limitations. Specifically, by updating the encoder parameters for a particular segmentation task and dataset, the VFM can no longer be used for any other downstream task. Each task and dataset require a separate ViT with finetuned parameters. As a consequence, if predictions are needed for multiple tasks or class definitions during deployment, one must either (a) maintain separate finetuned encoder-only models for each task, or (b) use a single frozen VFM encoder with inefficient task-specific decoders on top [41]. Clearly, both options are inefficient.

Therefore, in this work, we apply the philosophy pioneered by EoMT to the setting where the VFM is kept frozen. Specifically, given a frozen ViT encoder, we explore how much the task-specific decoders for image and video segmentation can be simplified when the ViT encoder is sufficiently large and pre-trained with large-scale data. While most task-specific modules could be removed without accuracy drop in the finetuned-encoder setting [20], we observe more substantial drops in combination with a frozen encoder. To compensate for this loss in accuracy without introducing substantial computational overhead, we present Plain Mask Transformer (PMT). PMT mimics the behavior of the last L_2 encoder layers of EoMT and VidEoMT with a small Transformer decoder, called the Plain Mask Decoder (PMD). This PMD takes the learnable queries and features from the frozen ViT encoder, and processes them jointly through regular Transformer layers, just like the last L_2 layers of EoMT. As this is a very lightweight module that only uses standard Transformer operations, this design preserves the architectural simplicity and low latency of encoder-only methods, while the encoder remains frozen and shareable across multiple downstream tasks. Importantly, this design seamlessly applies to both image and video segmentation, inheriting the generality of the encoder-only framework.

Through experiments, we find that PMT matches the accuracy of state-of-the-art frozen-encoder models for image segmentation while being up to $3\times$ faster. Moreover, for video segmentation, it can even compete or outperform *fully*

finetuned state-of-the-art methods, while being up to $8\times$ faster than frozen-encoder baselines. Together, these results demonstrate the effectiveness of PMT for image and video segmentation. Notably, PMT obtains these results while keeping the encoder frozen, making it directly compatible with multi-task deployment where a single shared encoder must serve multiple tasks simultaneously.

In summary, we make the following contributions.

- We identify and experimentally verify a fundamental limitation of encoder-only segmentation models: their approach of injecting learnable queries into the ViT encoder is not compatible with keeping the encoder frozen.
- To overcome this limitation, we propose the Plain Mask Decoder (PMD), a lightweight decoder that operates on frozen VFM features, reconciling the architectural simplicity and speed of encoder-only methods with the frozen-encoder paradigm. We term the resulting approach the Plain Mask Transformer (PMT).
- We find that PMT matches state-of-the-art frozen-encoder models on image segmentation while being up to $3\times$ faster, and that it performs on par with fully finetuned methods for video segmentation at speeds up to $8\times$ higher than frozen-encoder baselines.

2. Related Work

Image Segmentation. Image segmentation is a fundamental computer vision task that requires dividing an image into pixel-level segments, each associated with a class label. Traditionally, segmentation methods relied on per-pixel classification [7, 8, 28], assigning a label to each pixel.

Recently, the Mask Transformer paradigm [4, 10, 44] has enabled a unified mask-classification formulation for semantic, instance, and panoptic segmentation [22]. In this framework, a set of learnable object queries is refined through alternating self-attention among queries and cross-attention to image features in a Transformer decoder. Each processed query then predicts a class label via a linear layer and a binary segmentation mask via a dot product with the image features. Several works have been built on top of this framework to advance the state of the art in universal image segmentation [6, 11, 19, 24, 49]. To obtain competitive results, they typically combine a pre-trained encoder, a pixel decoder for multi-scale feature fusion, and a Transformer decoder for query-based mask and class prediction. When using large-scale pre-trained ViTs [39, 41] as encoders, models typically also include CNN-based adapter modules [9, 46] to recover multi-scale features.

More recently, EoMT [20] challenged the reliance on such task-specific components by demonstrating that, with sufficiently large and well-trained ViTs, these components are largely redundant: by directly injecting learnable queries into the last encoder layers, EoMT achieves competitive accuracy at a significantly higher inference speed.

Moreover, EoMT benefits from ongoing ViT advancements, such as Token Merging [3, 31, 37] and FlashAttention [12].

Video Segmentation. Video segmentation extends frame-level segmentation to the temporal domain, encompassing video instance segmentation (VIS) [48], video panoptic segmentation (VPS) [21], and video semantic segmentation (VSS) [36]. State-of-the-art methods [16, 23, 50, 51, 53] follow a decoupled paradigm: a per-frame segmenter produces masks and object queries, while a separate tracker associates them across time using specialized components such as context-aware feature extractors, re-identification layers, and temporal Transformer layers.

VidEoMT [38] recently extended EoMT’s encoder-only philosophy to video, showing that these tracking modules can be replaced by a lightweight query propagation mechanism used alongside the plain ViT encoder, achieving 5–10× speedups while preserving competitive accuracy. Crucially, both EoMT and VidEoMT require finetuning the full ViT encoder, preventing the encoder from being used for other downstream tasks. Our work directly addresses this limitation by moving query processing outside the encoder: we introduce a lightweight decoder that applies EoMT’s query-based attention mechanism on top of a fully frozen ViT, retaining the architectural simplicity and inference speed of the encoder-only approach while keeping the encoder features shareable across different downstream tasks.

3. Method

3.1. Preliminaries

Vision Transformer. A Vision Transformer [14] partitions an image $\mathbf{I} \in \mathbb{R}^{3 \times H \times W}$ into N non-overlapping patches of size $p \times p$, which are linearly projected into patch tokens $\mathbf{X}^0 \in \mathbb{R}^{D \times N}$. These tokens are then refined by L Transformer layers [43], where each layer l applies multi-head self-attention (MHSA) and a feed-forward network (FFN) with residual connections:

$$\begin{aligned} \mathbf{Z}^l &= \mathbf{X}^l + \text{MHSA}(\text{Norm}(\mathbf{X}^l)), \\ \mathbf{X}^{l+1} &= \mathbf{Z}^l + \text{FFN}(\text{Norm}(\mathbf{Z}^l)). \end{aligned} \quad (1)$$

where Norm denotes Layer Normalization [2]. The final tokens \mathbf{X}^L can be rearranged in a spatial grid to produce image features at $\frac{H}{p} \times \frac{W}{p}$ resolution.

EoMT. Traditional ViT-based segmentation models stack a CNN adapter [9], a pixel decoder, and a Transformer decoder [11] with masked cross-attention on top of the ViT encoder. EoMT [20] shows that, with strong VFM pre-training [39, 41] and sufficiently large model size, all these modules are largely redundant and can be removed, yielding large speedups at comparable accuracy. Instead of leveraging these task-specific modules, K learnable queries $\mathbf{Q}^{\text{lm}} = \{\mathbf{q}_i^{\text{lm}} \in \mathbb{R}^D\}_{i=1}^K$ are concatenated to the patch tokens after the first L_1 encoder layers. The last L_2 layers then

process the patch tokens and queries jointly as a single sequence. This means that the decoder’s MHSA operations, in which all tokens attend to all others, simultaneously conducts query self-attention and query-to-patch attention without an explicit cross-attention mechanism as typically used in Transformer decoders [11]. Finally, a lightweight mask module predicts, for each query, a class label using a linear layer and a segmentation mask through a dot product with patch tokens \mathbf{X}^L spatially reorganized and upsampled to resolution $\frac{H}{4} \times \frac{W}{4}$. During training, masked attention [11] is applied at each of the L_2 layers: an intermediate mask prediction is computed per query and used to restrict query-to-patch attention to the query’s predicted mask region, improving training convergence. However, in inference, predicting intermediate masks on every layer is expensive, and the custom attention pattern is incompatible with FlashAttention [12], which requires standard unmasked attention. To resolve this, *mask annealing* [20] gradually phases out masked attention during training, so the final model operates without any masking, unlocking FlashAttention, and roughly halving inference latency. Crucially, for EoMT, the *entire* encoder is finetuned, as the pre-trained attention must adapt to the newly introduced query tokens in order to produce meaningful query representations from which accurate segmentation predictions can be made.

VidEoMT. VidEoMT [38] extends EoMT to online video segmentation by replacing all task-specific tracking components [23, 50, 51] (tracker, context-aware features, re-identification layers) with a lightweight query-level temporal propagation mechanism. In the first frame ($t = 0$), the model operates identically to EoMT, taking learnable queries \mathbf{Q}^{lm} and producing output queries \mathbf{Q}_0 . In subsequent frames ($t > 0$), the output queries from the previous frame are fused with the learned queries through element-wise addition after a linear projection:

$$\mathbf{Q}_t^{\mathcal{F}} = \text{Linear}(\mathbf{Q}_{t-1}) + \mathbf{Q}^{\text{lm}}. \quad (2)$$

The fused queries $\mathbf{Q}_t^{\mathcal{F}}$ are then fed into the encoder instead of the learnable queries, carrying temporal context from the previous frame while retaining the ability to detect newly appearing objects. This design places all temporal reasoning in the query tokens and in the lightweight propagation module, avoiding slow task-specific modules. However, as with EoMT, the full encoder is finetuned.

Incompatibility with Frozen Encoders. In both EoMT and VidEoMT, queries are concatenated with patch tokens *inside* the encoder, after which both are processed by the *same* attention weights. Since pre-trained attention has no representation of these additional tokens, the weights must be updated for the joint patch-query attention to be effective. As a result, freezing the encoder does not merely reduce accuracy, it fundamentally prevents the mechanism from functioning, as the frozen MHSA has no means to

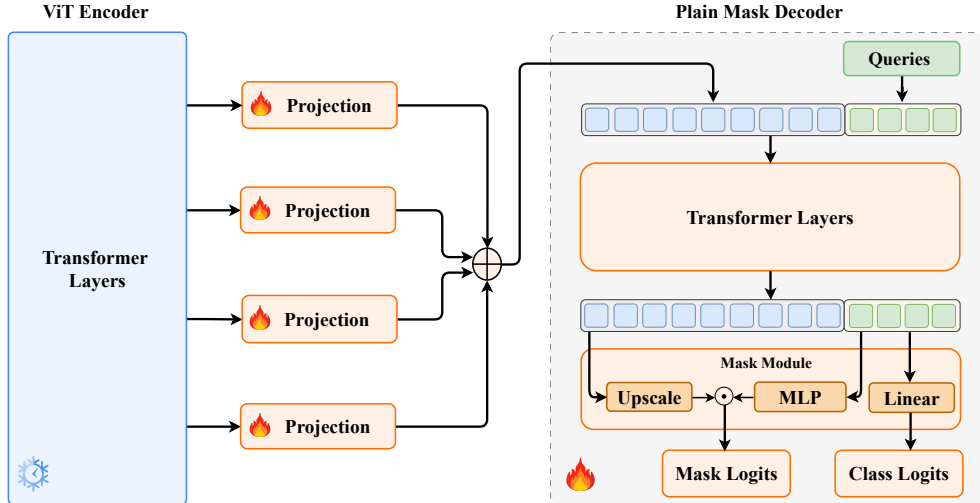


Figure 2. **Plain Mask Transformer (PMT) Architecture.** Instead of injecting the query tokens within the ViT encoder as in the encoder-only framework of EoMT and VidEoMT, we extract features at multiple encoder levels and feed them into an efficient segmentation decoder that processes queries and patch tokens in parallel. \oplus denotes element-wise addition. \odot denotes the dot product.

meaningfully attend to or from query tokens it was never trained on. We empirically verify this in Tab. 1: with a frozen decoder, using an encoder-only model results in a complete collapse of performance, confirming the specific incompatibility of EoMT’s joint patch-query attention with frozen weights. The same behavior applies in the video domain. Although this is not a limitation of the encoder-only design *per se*, it does make encoder-only models incompatible with the frozen-encoder paradigm for which large-scale VFMs are currently being designed [41].

3.2. Plain Mask Transformer Architecture

To enable efficient and accurate segmentation while using a frozen ViT encoder, our key insight is that the behavior of the last L_2 layers of EoMT’s encoder can be mimicked by small decoder consisting of the same types of layers. The application of this decoder, which we call the Plain Mask Decoder (PMD), allows the ViT encoder to remain frozen, preserving pre-training knowledge and enabling the ViT to serve any number of downstream tasks in parallel. The resulting model is called the Plain Mask Transformer (PMT).

Decoder Layers. The decoder contains vanilla Transformer layers that mirror the architecture of the DINOv3 encoder layers [41], matching the hidden dimension, the number of heads and the FFN design. Following EoMT, queries \mathbf{Q}^{lm} and patch tokens \mathbf{X}^L are concatenated into a single sequence and processed through standard MHSA: since all tokens attend to all others, this jointly achieves query self-attention, patch token self-attention, and attention between queries and patches in both directions, just like EoMT. Unlike EoMT, however, these are standalone layers trained from randomly initialized weights, while the encoder weights remain entirely frozen. We use $L_d = 6$

decoder layers by default (see Tab. 5).

Following EoMT, masked attention [11] is applied during training in each decoder layer, forcing each query to attend to its predicted region. Mask annealing [20] then progressively phases out this masking, yielding a consistently faster mask-free decoder at inference. We denote the set of decoder output queries as $\hat{\mathbf{Q}} = \{\hat{\mathbf{q}}_i \in \mathbb{R}^D\}_{i=1}^K$ and the decoder output patch tokens as $\hat{\mathbf{X}} \in \mathbb{R}^{D \times N}$.

Mask Module. We adopt the same prediction head as EoMT and VidEoMT. For each output query $\hat{\mathbf{q}}_i \in \hat{\mathbf{Q}}$, class logits $\mathbf{c}_i \in \mathbb{R}^C$ are predicted by a linear layer. Mask logits $\mathbf{M}_i \in \mathbb{R}^{\frac{H}{4} \times \frac{W}{4}}$ are obtained by first applying a three-layer MLP to $\hat{\mathbf{q}}_i$, then taking its dot product with $\mathbf{X}^{\text{up}} \in \mathbb{R}^{D \times \frac{H}{4} \times \frac{W}{4}}$, obtained after reshaping and upscaling $\hat{\mathbf{X}}$.

Lateral Connections. When EoMT is finetuned, the early L_1 encoder layers can adapt to the target task producing features that are more useful for the query-processing layers that follow. A frozen encoder cannot do this: its features are fixed and not adapted to the target task. As a consequence, the final encoder output \mathbf{X}^L may not contain all cues that are useful for segmentation (*e.g.*, edges, boundaries), even though these may be available in features of earlier layers.

Analogously to how adapters [9] extract multi-scale features at selected encoder depths, we introduce lateral connections that collect patch tokens \mathbf{X}^l from evenly spaced encoder layers (including the final layer L). This allows the decoder to leverage the rich information available at different encoder depths, improving the quality of the mask predictions. For normalization, we follow the strategy that the DINOv3 [41] paper uses when feeding intermediate features to the decoder for downstream tasks. Specifically, we apply the encoder’s final Layer Normalization [2] to all extracted token features, followed by a trainable Batch Nor-

malization [18] layer. All token features are then projected by a two-layer MLP with a residual connection. Features from all branches are summed element-wise into a single multi-depth representation that serves as the set of patch tokens that is fed into the decoder.

Positional Encoding. DINOv3 [41] employs Rotary Position Embeddings (RoPE) [42] in every encoder layer, encoding relative spatial positions directly into the attention computation by rotating queries and keys before the dot product. Since our decoder uses its own freshly initialized attention layers, applying the same RoPE provides them with explicit spatial context, supplementing the positional information already embedded in the patch tokens.

We therefore apply RoPE to the decoder layers: patch tokens retain the grid coordinates assigned by the encoder, while query tokens receive no positional encoding, as keeping them position-free preserves the permutation-invariant nature of the set of object queries. Their spatial grounding is provided implicitly through attention to positioned patches and through the mask module. This adds no learnable parameters, as RoPE is a deterministic function of position.

3.3. Temporal Modeling

Our approach extends naturally to online video segmentation by adopting VidEoMT’s query propagation mechanism [38]. Each frame is processed independently by the frozen encoder and lateral connections; the only temporal link is found in the queries fed to the decoder.

At $t = 0$ the decoder receives the learnable queries Q^{lm} . In subsequent frames ($t > 0$), the output queries of the previous frame are fused with the learnable queries following Eq. (2) and fed to the PMD decoder. As in VidEoMT, no tracker, re-identification layers, or context-aware features are needed, yielding a simple and fast video architecture.

4. Experiments

4.1. Experimental Setup

Unless stated otherwise, we follow the experimental setup of EoMT [20] for image-level experiments and VidEoMT [38] for video-level experiments.

Datasets. For image segmentation, we use COCO [25] for panoptic and instance segmentation, and ADE20K [52] for semantic segmentation. For video, we use YouTube-VIS 2019 and 2021 [47] for video instance segmentation (VIS), VIPSeg [34] for video panoptic segmentation (VPS), and VSPW [33] for video semantic segmentation (VSS).

Models. Unless stated otherwise, we use DINOv3-L [41] as the encoder with a patch size of 16×16 and a 640×640 resolution. Our PMD matches the hidden dimension of the encoder to avoid information bottlenecks. Register and class tokens are propagated together with the patch tokens through the decoder layers, and the MLP expansion factors

Method	Params	GFLOPs	FPS	PQ
(0) ViT-Adapter + Mask2Former	340M	804	48	56.4
(1) \hookrightarrow w/o ViT-Adapter	341M	740	62	54.0
(2) \hookrightarrow w/o Pixel decoder	336M	686	77	52.9
(3) \hookrightarrow w/o Multi-scale	327M	673	81	52.0
(4) \hookrightarrow w/o Transformer decoder = EoMT	315M	668	162	6.8

Table 1. **From ViT-Adapter + Mask2Former to EoMT.** Stepwise removal of Mask2Former modules toward EoMT with *frozen* DINOv3 [41] encoder. Evaluated on COCO *val2017* [25].

are set to 1. For ViT-Adapter, we follow the implementation from the DINOv3 paper [41], removing the injectors to preserve the frozen encoder representation and adding a learnable Batch Normalization [18] layer at each feature level. At inference, the QKV projections within the MHSA layers of the encoder and decoder are fused to reduce latency.

Training. All models are trained in mixed precision with AdamW [30] and mask annealing following EoMT with DINOv3. For image models, we use a batch size of 16, a learning rate of 2×10^{-4} , cosine annealing scheduler [29], and training schedules of 12 and 16 epochs on COCO and ADE20K, respectively. For video models, we use a batch size of 8 with a 5-frame temporal window, a learning rate of 10^{-4} , polynomial learning rate decay with a power of 0.9, and training iterations and resolutions following CAVIS [23]. In both settings, we apply linear warmup for 6000 iterations. Following common practice [11, 20, 38], we use cross-entropy for classification and binary cross-entropy combined with Dice loss [35] for mask prediction. For video, ground-truth matching follows VidEoMT: each object is matched to a query in its first appearing frame, and the assignment persists across subsequent frames.

Evaluation. For image segmentation, we report Panoptic Quality (PQ) [22] for panoptic, mean Intersection over Union (mIoU) for semantic, and Average Precision (AP) [25] for instance segmentation. For video segmentation, we report AP and Average Recall (AR) [47] for VIS, Video Panoptic Quality (VPQ) [21] and Segmentation and Tracking Quality (STQ) [45] for VPS, and mIoU along with Video Consistency (mVC) [33] for VSS. Inference speed (FPS) is measured on an NVIDIA H100 GPU with FlashAttention-2 [12] and `torch.compile` [1] enabled, using a batch size of 1 and automatic mixed precision. We set `torch.compile` to *max-autotune* mode for image experiments and use the default settings for video experiments due to varying resolutions. GFLOPs are computed using *fvcore* [32]. Both FPS and GFLOPs are measured by averaging across the validation sets.

4.2. Main Results

From ViT-Adapter + Mask2Former to EoMT. In Tab. 1, we evaluate the stepwise removal of the task-specific components from the state-of-the-art ViT-Adapter

Method	Params	GFLOPs	FPS	PQ
<i>DINOv3 pre-training</i>				
(0) EoMT [20]	316M	668	162	6.8
(1) \hookrightarrow w/ plain decoder	354M	762	145	53.7
(2) \hookrightarrow w/ lateral connections	357M	767	142	55.9
(3) \hookrightarrow w/ RoPE = PMT (Ours)	357M	767	141	56.1
<i>DINOv2 pre-training</i>				
(0) EoMT [20]	317M	668	172	22.3
(1) \hookrightarrow w/ plain decoder	356M	762	150	51.4
(2) \hookrightarrow w/ lateral connections	359M	767	148	55.0
(3) \hookrightarrow w/ RoPE = PMT (Ours)	359M	767	146	55.5

Table 2. **From EoMT to PMT.** Stepwise addition of modules from EoMT with *frozen* DINOv3 [41] and DINOv2 [39] encoders to our PMT. Evaluated on COCO *val2017* [25].

+ Mask2Former [9, 11] model toward the EoMT encoder-only design with a frozen DINOv3 encoder. Steps (1)–(3) strip the adapter, pixel decoder, and multi-scale processing successively, dropping PQ from 56.4 to 52.0 while nearly doubling FPS. Unlike in the original EoMT results where these modules proved largely redundant under full encoder fine-tuning, the frozen setting exposes a clear accuracy loss: the remaining trainable parameters lack the capacity to compensate for the removed components when the encoder cannot adapt. Step (4) reaches the encoder-only EoMT configuration and, despite doubling again the speed, causes a far more severe collapse to 6.8 PQ. Interestingly, this drop is disproportionate compared to any earlier step, highlighting the failure of joint patch-query attention when keeping weights frozen, as discussed in Sec. 3.

From EoMT with Frozen Encoder to PMT. In Tab. 2, we build up from the collapsed frozen EoMT baseline to our PMT. Step (1) adds a standalone PMD and immediately closes most of the gap, reaching 53.7 PQ with DINOv3 while only reducing inference speed by a small margin. Step (2) incorporates lateral connections that fuse patch tokens collected at evenly spaced encoder depths, adding a further 2.2 PQ to reach 55.9 PQ at very little computational cost. Step (3) applies RoPE to the decoder, yielding the full PMT model at 56.1 PQ, a +0.2 PQ gain at virtually no cost, as RoPE introduces minimal latency and no additional learnable parameters. Comparable trends hold for DINOv2, although the gains from lateral connections and RoPE over the plain decoder are more pronounced, with +3.6 and +0.5 PQ, respectively. This is consistent with EoMT’s observation [20] that stronger pre-training reduces the necessity for additional components. Overall, these results show that processing queries with our lightweight decoder and lateral connections is sufficient to recover almost all of the performance of the baseline with complex task-specific modules, while being 3 \times faster (*cf.* Tab. 1).

Impact of Pre-training. Next, we examine how the extent of pre-training affects the performance of PMT in Tab. 3. We evaluate DINOv3 [41] and DINOv2 [39] as large-scale

Model	Pre-train	Params	GFLOPs	FPS	PQ
ViT-Adapter + M2F	DINOv3	340M	804	48	56.4
PMT (Ours)		357M	767	141	56.1
ViT-Adapter + M2F	DINOv2	342M	804	49	55.7
PMT (Ours)		359M	767	146	55.5
ViT-Adapter + M2F	IN21K	342M	804	49	51.0
PMT (Ours)		359M	767	146	49.7
ViT-Adapter + M2F	IN1K	342M	804	49	47.0
PMT (Ours)		359M	767	146	44.6

Table 3. **Pre-training.** Impact of pre-training on segmentation quality. Evaluated on COCO *val2017* [25].

Model	Size	Params	GFLOPs	FPS	PQ
ViT-Adapter + M2F	L	340M	804	48	56.4
PMT (Ours)		357M	767	141	56.1
ViT-Adapter + M2F	B	116M	334	64	53.6
PMT (Ours)		116M	281	262	52.8
ViT-Adapter + M2F	S	45M	163	73	49.6
PMT (Ours)		29M	91	400	45.3

Table 4. **Model Size.** Impact of model size on segmentation quality and inference speed. Evaluated on COCO *val2017* [25].

Blocks	Params	GFLOPs	FPS	PQ
2	332M	695	153	54.0
4	344M	731	146	55.6
6	357M	767	141	56.1
8	370M	803	133	56.1

Table 5. **Decoder Layers.** Impact of number of decoder layers on segmentation quality and inference speed. Evaluated on COCO *val2017* [25].

self-supervised models, as well as encoders trained in supervised fashion on ImageNet-21K [13] and ImageNet-1K [40]. The results show that large-scale pre-training is essential for PMT to close the gap with ViT-Adapter + M2F. The accuracy difference with DINOv3 and DINOv2 is just 0.3 and 0.2 PQ, respectively, while the gap increases to 1.3 PQ under ImageNet-21K supervision and 2.4 PQ under ImageNet-1K. The widening gap at less extensive pre-training confirms that the frozen encoder must carry sufficiently rich features for the lightweight PMD to substitute complex task-specific modules, which is in line with the scaling observations of EoMT [20] and VidEoMT [38].

Impact of Model Size. Tab. 4 extends the comparison to different model sizes. While the accuracy gap between PMT and ViT-Adapter + M2F reaches 4.3 PQ with the small ViT-S model, it narrows to 0.8 PQ with ViT-B and decreases to just 0.3 PQ with ViT-L. This scaling pattern confirms that PMD requires a frozen encoder with sufficient capacity to compensate for the absence of dedicated feature-adaptation modules. Importantly, these results also show that PMT delivers considerably higher inference speed across all sizes, with $\sim 3\times$ at ViT-L. In fact, ViT-L is even faster than ViT-Adapter + M2F at ViT-S at much greater accuracy, demonstrating PMT’s superior accuracy–efficiency trade-off.

Method	Backbone	Pre-training	Encoder	Input size	Params	GFLOPs	FPS	PQ	AP
Mask2Former [†] [11]	Swin-L [26]	IN21K	🔥	800 ²	216M	868	24	57.8	50.1
kMaX-DeepLab [49]	ConvNext-L [27]	IN21K	🔥	1281 ²	232M	–	–	58.0	–
OneFormer [†] [19]	DiNAT-L [15]	IN21K	🔥	800 ²	223M	736	20	58.0	49.2
MaskDINO [†] [24]	Swin-L [26]	IN21K	🔥	800 ²	223M	1326	14	58.3	52.3
EoMT [20]	ViT-L [14]	DINOv2	🔥	640 ²	316M	669	172	56.0	45.2
EoMT [20]	ViT-L [14]	DINOv3	🔥	640 ²	315M	668	162	56.8	45.9
EoMT [20]	ViT-L [14]	DINOv2	🔥	1280 ²	322M	4146	35	58.3	48.8
EoMT [20]	ViT-L [14]	DINOv3	🔥	1280 ²	315M	4144	34	58.9	49.9
Mask2Former [11]	ViT-Adapter-L [9]	DINOv2	❄️	640 ²	342M	804	49	55.7	45.0
Mask2Former [11]	ViT-Adapter-L [9]	DINOv3	❄️	640 ²	340M	804	48	56.4	45.9
PMT (Ours)	ViT-L [14]	DINOv2	❄️	640 ²	359M	767	146	55.5	44.4
PMT (Ours)	ViT-L [14]	DINOv3	❄️	640 ²	357M	767	141	56.1	45.4
Mask2Former [11]	ViT-Adapter-L [9]	DINOv2	❄️	1280 ²	347M	4711	16	56.6	47.6
Mask2Former [11]	ViT-Adapter-L [9]	DINOv3	❄️	1280 ²	340M	4711	15	58.1	50.0
PMT (Ours)	ViT-L [14]	DINOv2	❄️	1280 ²	364M	4925	30	56.1	45.9
PMT (Ours)	ViT-L [14]	DINOv3	❄️	1280 ²	357M	4925	29	58.1	49.0

Table 6. **PMT for Panoptic and Instance Segmentation on COCO val2017 [25]**. [†]During inference, these models resize the shortest side of images to the indicated scale, while preserving the aspect ratio.

Method	Backbone	Pre-training	Encoder	Input size	Params	GFLOPs	FPS	mIoU
Mask2Former [†] [11]	Swin-L [26]	IN21K	🔥	640 ²	216M	–	33	56.1
MaskDINO [†] [24]	Swin-L [26]	IN21K	🔥	640 ²	223M	–	–	56.6
OneFormer [†] [19]	ConvNext-XL [27]	IN21K	🔥	640 ²	373M	607	21	57.4
OneFormer [†] [19]	DiNAT-L [15]	IN21K	🔥	896 ²	223M	678	19	58.1
EoMT [20]	ViT-L [14]	DINOv2	🔥	512 ²	316M	721	154	58.4
EoMT [20]	ViT-L [14]	DINOv3	🔥	512 ²	315M	721	151	59.5
Mask2Former [11]	ViT-Adapter-L [9]	DINOv2	❄️	512 ²	341M	879	41	57.5
PMT (Ours)	ViT-L [14]	DINOv2	❄️	512 ²	358M	823	135	57.2
Mask2Former [11]	ViT-Adapter-L [9]	DINOv3	❄️	512 ²	340M	879	40	58.7
PMT (Ours)	ViT-L [14]	DINOv3	❄️	512 ²	357M	823	128	58.5

Table 7. **PMT for Semantic Segmentation on ADE20K [52]**. [†]These models resize the shortest side of images to the indicated scale during inference, while preserving the aspect ratio.

Number of Decoder Layers. In Tab. 5, we evaluate how the depth of the decoder affects accuracy and speed. Increasing from 2 to 4 layers brings a consistent improvement from 54.0 to 55.6 PQ, and 6 layers add a further 0.5 PQ to reach 56.1 PQ. Beyond that, scaling up to 8 layers yields no additional gain. Performance thus saturates quickly with depth, showing that a shallow decoder is sufficient for this design. We therefore set $L_d=6$ as the default.

4.3. Image Segmentation Benchmarks

Panoptic and Instance Segmentation. In Tab. 6, we compare PMT with state-of-the-art panoptic and instance segmentation methods on COCO. Compared to the state-of-the-art frozen-encoder method that uses task-specific components (ViT-Adapter + Mask2Former), PMT obtains comparable performance at much higher speed. PMT scores only 0.3 PQ and 0.5 AP lower at 640² resolution, but is $\sim 3\times$ faster. This demonstrates PMT’s effectiveness and efficiency. Compared to the encoder-only EoMT, which *does* fully finetune the encoder, PMT obtains only slightly lower accuracy and speeds, with a 0.7 PQ difference and 13% speed decrease at 640². Remarkably, PMT achieves this while keeping the encoder frozen, making it much more

suitable for applications that require reusing the frozen encoder for multiple downstream tasks.

Semantic Segmentation. In Tab. 7, we evaluate PMT for semantic segmentation on ADE20K. Compared to ViT-Adapter + Mask2Former with a frozen encoder, PMT obtains almost the same segmentation accuracy, with drops of only 0.3 and 0.2 mIoU in combination with DINOv2 and DINOv3, respectively. Once again, PMT is considerably faster, with inference speed gains of more than $3\times$, at 128 vs. 40 FPS. Like for panoptic and instance segmentation, EoMT with a finetuned encoder performs slightly better than PMT, but the accuracy drop remains modest at 1.0 or 1.2 mIoU. Of course, PMT obtains these scores without finetuning the encoder, improving its applicability. Together, these results confirm that the earlier observed accuracy and efficiency advantages also extend to semantic segmentation, demonstrating the generality of PMT’s design.

4.4. Video Segmentation Benchmarks

Video Instance Segmentation. In Tab. 8, we compare PMT with state-of-the-art online VIS models on YouTube-VIS 2019 and 2021. Here, the baseline frozen-encoder model that we compare to is CAVIS [23], a state-of-the-

Method	Backbone	Pre-training	Encoder	YouTube-VIS 2019 <i>val</i> [47]					YouTube-VIS 2021 <i>val</i> [47]				
				GFLOPs	FPS	AP	AP ₇₅	AR ₁₀	GFLOPs	FPS	AP	AP ₇₅	AR ₁₀
MinVIS [17]	Swin-L [26]	IN21K	🔥	401	29	61.6	68.6	66.6	255	30	55.3	62.0	60.8
DVIS [50]	Swin-L [26]	IN21K	🔥	411	23	63.9	70.4	69.0	405	24	58.7	66.6	64.6
DVIS-DAQ [53]	Swin-L [26]	IN21K	🔥	415	13	65.7	73.6	70.7	410	11	61.1	68.2	66.6
DVIS++ [51]	ViT-Adapter-L [9]	DINOv2	🔥	846	18	67.7	75.3	73.7	830	17	62.3	70.2	68.0
DVIS-DAQ [53]	ViT-Adapter-L [9]	DINOv2	🔥	851	10	68.3	76.1	73.5	836	10	62.4	70.8	68.0
CAVIS [23]	ViT-Adapter-L [9]	DINOv2	🔥	838	15	68.9	76.2	73.6	824	15	64.6	72.5	69.3
VidEoMT [38]	ViT-L [14]	DINOv2	🔥	566	160	68.6	75.6	73.9	560	160	63.1	69.3	68.1
VidEoMT [38]	ViT-L [14]	DINOv3	🔥	566	133	68.9	77.4	74.8	560	133	63.2	71.6	69.1
CAVIS [23]	ViT-Adapter-L [9]	DINOv2	❄️	838	15	68.5	75.8	73.5	824	15	64.3	72.0	68.9
PMT (Ours)	ViT-L [14]	DINOv2	❄️	617	124	68.8	75.2	73.9	616	124	63.8	69.4	68.1
CAVIS [23]	ViT-Adapter-L [9]	DINOv3	❄️	838	13	68.8	75.6	73.3	824	13	63.9	71.6	68.2
PMT (Ours)	ViT-L [14]	DINOv3	❄️	617	113	69.2	76.5	74.6	616	113	64.3	71.2	69.0

Table 8. **PMT for Online VIS on YouTube-VIS 2019 and 2021 [47].**

Method	Backbone	PT	Encoder	VIPSeg <i>val</i> [34]			
				GFLOPs	FPS	VPQ	STQ
DVIS [50]	Swin-L [26]	I	🔥	879	20	54.7	47.7
DVIS++ [51]	ViT-Adapter-L [9]	D2	🔥	2290	13	56.0	49.8
DVIS-DAQ [53]	ViT-Adapter-L [9]	D2	🔥	2315	4	57.4	52.0
CAVIS [23]	ViT-Adapter-L [9]	D2	🔥	2612	10	56.9	51.0
VidEoMT [38]	ViT-L [14]	D2	🔥	1897	75	55.2	48.9
VidEoMT [38]	ViT-L [14]	D3	🔥	1897	71	55.1	48.1
CAVIS [23]	ViT-Adapter-L [9]	D2	❄️	2612	10	56.4	49.0
PMT (Ours)	ViT-L [14]	D2	❄️	2037	60	55.3	48.2
CAVIS [23]	ViT-Adapter-L [9]	D3	❄️	2612	9	56.8	51.2
PMT (Ours)	ViT-L [14]	D3	❄️	2037	58	55.5	49.2

Table 9. **PMT for Online VPS on VIPSeg [21]. PT:** Pre-training. **I:** ImageNet-21K [13]. **D2:** DINOv2 [39]. **D3:** DINOv3 [41].

Method	Backbone	PT	Encoder	VSPW <i>val</i> [33]			
				GFLOPs	FPS	mVC ₁₆	mIoU
DVIS [50]	Swin-L [26]	I	🔥	879	22	94.3	61.3
DVIS++ [51]	ViT-Adapter-L [9]	D2	🔥	2290	13	94.2	62.8
VidEoMT [38]	ViT-L [14]	D2	🔥	1909	73	95.0	64.9
VidEoMT [38]	ViT-L [14]	D3	🔥	1909	71	94.4	64.0
PMT (Ours)	ViT-L [14]	D2	❄️	2049	60	94.6	64.3
PMT (Ours)	ViT-L [14]	D3	❄️	2049	57	94.9	65.7

Table 10. **PMT for Online VSS on VSPW [33]. PT:** Pre-training. **I:** ImageNet-21K [13]. **D2:** DINOv2 [39]. **D3:** DINOv3 [41].

art model with many task-specific components that performs well when keeping the backbone frozen. Compared to CAVIS, PMT obtains consistent speed gains of more than $8\times$, which are even larger than those observed for image segmentation, as video segmentation models use additional inefficient components. For this task, PMT also consistently obtains a slightly higher accuracy than CAVIS when using a DINOv3 encoder, with 69.2 vs. 68.8 mAP for Youtube-VIS 2019. Notably, PMT even performs better than the state-of-the-art CAVIS and VidEoMT models that *finetune* the encoder, while being only slightly slower than VidEoMT. These results demonstrate the strength of PMT’s design for video segmentation, as they show that it can obtain state-of-the-art results at high inference speeds, while still allowing the frozen encoder to be reused for other tasks.

Video Panoptic Segmentation. In Tab. 9, we compare PMT with state-of-the-art VPS methods on VIPSeg. As in

the video instance segmentation setting, PMT is substantially faster than the frozen-encoder CAVIS model. In this case, PMT’s accuracy is slightly lower, with gaps of up to 1.3 VPQ, which we expect to be due to the higher complexity of the VPS task. Again, however, PMT performs better than VidEoMT that finetunes the encoder, while only being slightly slower. These results offer further evidence of the effectiveness of PMT and its favorable accuracy vs. efficiency trade-off.

Video Semantic Segmentation. In Tab. 10, we evaluate PMT for video semantic segmentation on VSPW. Notably, Plain Mask Transformer obtains new state-of-the-art results on this dataset in terms of the main mIoU metric, with 65.7 vs. the prior best of 64.9 . Impressively, this is obtained while keeping the encoder frozen. This further demonstrates the strength of PMT’s design.

5. Conclusion

In this work, we reconcile the architectural simplicity and speed of encoder-only segmentation models with the practical need to keep Vision Foundation Model encoders frozen. Our Plain Mask Decoder (PMD) achieves this by replicating the joint query-patch attention of EoMT’s last encoder blocks in a small module that operates entirely on top of frozen features. The resulting model, Plain Mask Transformer (PMT), applies seamlessly to both image and video segmentation: on standard image benchmarks it matches the frozen-encoder state of the art at up to $\sim 3\times$ higher inference speed, while on video benchmarks it achieves accuracies on par with fully finetuned methods, at up to $8\times$ the speed of state-of-the-art frozen-encoder baselines. Our ablations confirm that the effectiveness of the lightweight PMD depends on a sufficiently large and extensively pre-trained encoder, in line with the scaling observations of EoMT [20] and VidEoMT [38]. Because the encoder remains entirely untouched, Plain Mask Transformer enables efficient multi-task deployment where a single shared frozen encoder serves multiple downstream tasks and datasets simultaneously.

Acknowledgements. This work was partly funded by the Cynergy4MIE project, which is supported by the Chips Joint Undertaking and its members, including the top-up funding by National Authorities under Grant Agreement No 101140226.

References

- [1] Jason Ansel, Edward Yang, Horace He, Natalia Gimelshein, Animesh Jain, Michael Voznesensky, Bin Bao, Peter Bell, David Berard, Evgeni Burovski, Geeta Chauhan, Anjali Chourdia, Will Constable, Alban Desmaison, Zachary DeVito, Elias Ellison, Will Feng, Jiong Gong, Michael Gschwind, Brian Hirsh, Sherlock Huang, Kshiteej Kalambarkar, Laurent Kirsch, Michael Lazos, Mario Lezcano, Yanbo Liang, Jason Liang, Yinghai Lu, C. K. Luk, Bert Maher, et al. PyTorch 2: Faster machine learning through dynamic python bytecode transformation and graph compilation. In *ASPLOS*, 2024. 5
- [2] Jimmy Lei Ba, Jamie Ryan Kiros, and Geoffrey E. Hinton. Layer normalization. *arXiv preprint arXiv:1607.06450*, 2016. 3, 4
- [3] Daniel Bolya, Cheng-Yang Fu, Xiaoliang Dai, Peizhao Zhang, Christoph Feichtenhofer, and Judy Hoffman. Token merging: Your ViT but faster. In *ICLR*, 2023. 3
- [4] Nicolas Carion, Francisco Massa, Gabriel Synnaeve, Nicolas Usunier, Alexander Kirillov, and Sergey Zagoruyko. End-to-end object detection with transformers. In *ECCV*, 2020. 2
- [5] Mathilde Caron, Hugo Touvron, Ishan Misra, Hervé Jégou, Julien Mairal, Piotr Bojanowski, and Armand Joulin. Emerging properties in self-supervised vision transformers. In *ICCV*, 2021. 1
- [6] Niccolò Cavagnero, Gabriele Rosi, Claudia Cuttano, Francesca Pistilli, Marco Ciccone, Giuseppe Averta, and Fabio Cermelli. PEM: Prototype-based efficient MaskFormer for image segmentation. In *CVPR*, 2024. 2
- [7] Liang-Chieh Chen, George Papandreou, Iasonas Kokkinos, Kevin Murphy, and Alan L. Yuille. DeepLab: Semantic image segmentation with deep convolutional nets, atrous convolution, and fully connected CRFs. *IEEE TPAMI*, 40(4): 834–848, 2018. 2
- [8] Liang-Chieh Chen, Yukun Zhu, George Papandreou, Florian Schroff, and Hartwig Adam. Encoder-decoder with atrous separable convolution for semantic image segmentation. In *ECCV*, 2018. 2
- [9] Zhe Chen, Yuchen Duan, Wenhai Wang, Junjun He, Tong Lu, Jifeng Dai, and Yu Qiao. Vision transformer adapter for dense predictions. In *ICLR*, 2023. 1, 2, 3, 4, 6, 7, 8
- [10] Bowen Cheng, Alex Schwing, and Alexander Kirillov. Per-pixel classification is not all you need for semantic segmentation. In *NeurIPS*, 2021. 1, 2
- [11] Bowen Cheng, Ishan Misra, Alexander G. Schwing, Alexander Kirillov, and Rohit Girdhar. Masked-attention mask transformer for universal image segmentation. In *CVPR*, 2022. 1, 2, 3, 4, 5, 6, 7
- [12] Tri Dao. FlashAttention-2: Faster attention with better parallelism and work partitioning. In *ICLR*, 2024. 3, 5
- [13] Jia Deng, Wei Dong, Richard Socher, Li-Jia Li, Kai Li, and Li Fei-Fei. ImageNet: A large-scale hierarchical image database. In *CVPR*, 2009. 6, 8
- [14] Alexey Dosovitskiy, Lucas Beyer, Alexander Kolesnikov, Dirk Weissenborn, Xiaohua Zhai, Thomas Unterthiner, Mostafa Dehghani, Matthias Minderer, Georg Heigold, Sylvain Gelly, Jakob Uszkoreit, and Neil Houlsby. An image is worth 16x16 words: Transformers for image recognition at scale. In *ICLR*, 2021. 1, 3, 7, 8
- [15] Ali Hassani and Humphrey Shi. Dilated neighborhood attention transformer. *arXiv preprint arXiv:2209.15001*, 2022. 7
- [16] Miran Heo, Sukjun Hwang, Jeongseok Hyun, Hanjung Kim, Seoung Wug Oh, Joon-Young Lee, and Seon Joo Kim. A Generalized Framework for Video Instance Segmentation. In *CVPR*, 2023. 3
- [17] De-An Huang, Zhiding Yu, and Anima Anandkumar. Min-VIS: A minimal video instance segmentation framework without video-based training. In *NeurIPS*, 2022. 8
- [18] Sergey Ioffe and Christian Szegedy. Batch Normalization: Accelerating Deep Network Training by Reducing Internal Covariate Shift. 2015. 5
- [19] Jitesh Jain, Jiachen Li, Mang Tik Chiu, Ali Hassani, Nikita Orlov, and Humphrey Shi. OneFormer: One transformer to rule universal image segmentation. In *CVPR*, 2023. 1, 2, 7
- [20] Tommie Kerssies, Niccolò Cavagnero, Alexander Hermans, Narges Norouzi, Giuseppe Averta, Bastian Leibe, Gijs Dubbelman, and Daan de Geus. Your ViT is secretly an image segmentation model. In *CVPR*, 2025. 1, 2, 3, 4, 5, 6, 7, 8
- [21] Dahun Kim, Sanghyun Woo, Joon-Young Lee, and In So Kweon. Video panoptic segmentation. In *CVPR*, 2020. 3, 5, 8
- [22] Alexander Kirillov, Kaiming He, Ross Girshick, Carsten Rother, and Piotr Dollár. Panoptic segmentation. In *CVPR*, 2019. 2, 5
- [23] Seunghun Lee, Jiwan Seo, Kiljoon Han, Minwoo Choi, and Sunghoon Im. Context-aware video instance segmentation. In *ICCV*, 2025. 3, 5, 7, 8
- [24] Feng Li, Hao Zhang, Huaizhe Xu, Shilong Liu, Lei Zhang, Lionel M. Ni, and Heung-Yeung Shum. Mask DINO: Towards a unified transformer-based framework for object detection and segmentation. In *CVPR*, 2023. 2, 7
- [25] Tsung-Yi Lin, Michael Maire, Serge Belongie, James Hays, Pietro Perona, Deva Ramanan, Piotr Dollár, and C. Lawrence Zitnick. Microsoft COCO: Common objects in context. In *ECCV*, 2014. 1, 5, 6, 7
- [26] Ze Liu, Yutong Lin, Yue Cao, Han Hu, Yixuan Wei, Zheng Zhang, Stephen Lin, and Baining Guo. Swin transformer: Hierarchical vision transformer using shifted windows. In *ICCV*, 2021. 7, 8
- [27] Zhuang Liu, Hanzi Mao, Chao-Yuan Wu, Christoph Feichtenhofer, Trevor Darrell, and Saining Xie. A ConvNet for the 2020s. In *CVPR*, 2022. 7
- [28] Jonathan Long, Evan Shelhamer, and Trevor Darrell. Fully convolutional networks for semantic segmentation. In *CVPR*, 2015. 2

- [29] Ilya Loshchilov and Frank Hutter. SGDR: Stochastic Gradient Descent with Warm Restarts. In *ICLR*, 2017. 5
- [30] Ilya Loshchilov and Frank Hutter. Decoupled weight decay regularization. In *ICLR*, 2019. 5
- [31] Chenyang Lu, Daan de Geus, and Gijs Dubbelman. Content-Aware Token Sharing for Efficient Semantic Segmentation With Vision Transformers. In *CVPR*, 2023. 3
- [32] Meta Research. fvcore, 2023. 5
- [33] Jiaxu Miao, Yunchao Wei, Yu Wu, Chen Liang, Guangrui Li, and Yi Yang. VSPW: A Large-scale Dataset for Video Scene Parsing in the Wild. In *CVPR*, 2021. 5, 8
- [34] Jiaxu Miao, Xiaohan Wang, Yu Wu, Wei Li, Xu Zhang, Yunchao Wei, and Yi Yang. Large-Scale Video Panoptic Segmentation in the Wild: A Benchmark. In *CVPR*, 2022. 5, 8
- [35] Fausto Milletari, Nassir Navab, and Seyed-Ahmad Ahmadi. V-Net: Fully convolutional neural networks for volumetric medical image segmentation. In *3DV*, 2016. 5
- [36] David Nilsson and Cristian Sminchisescu. Semantic video segmentation by gated recurrent flow propagation. In *CVPR*, 2018. 3
- [37] Narges Norouzi, Svetlana Orlova, Daan de Geus, and Gijs Dubbelman. ALGM: Adaptive local-then-global token merging for efficient semantic segmentation with plain vision transformers. In *CVPR*, 2024. 3
- [38] Narges Norouzi, Idil Esen Zulfikar, Niccolò Cavagnero, Tommie Kerssies, Bastian Leibe, Gijs Dubbelman, and Daan de Geus. VidEoMT: Your ViT is secretly also a video segmentation model. In *CVPR*, 2026. 1, 2, 3, 5, 6, 8
- [39] Maxime Oquab, Timothée Darcet, Théo Moutakanni, Huy Vo, Marc Szafraniec, Vasil Khalidov, Pierre Fernandez, Daniel Haziza, Francisco Massa, Alaaeldin El-Nouby, et al. DINOv2: Learning robust visual features without supervision. *TMLR*, 2024. 1, 2, 3, 6, 8
- [40] Olga Russakovsky, Jia Deng, Hao Su, Jonathan Krause, Sanjeev Satheesh, Sean Ma, Zhiheng Huang, Andrej Karpathy, Aditya Khosla, Michael Bernstein, et al. ImageNet large scale visual recognition challenge. *IJCV*, 2015. 6
- [41] Oriane Siméoni, Huy V. Vo, Moritz Seitzer, Filippo Baldassarre, Maxime Oquab, Camille Jose, Vasil Khalidov, Marc Szafraniec, Souyoung Yi, Manu Ramamonjisoa, Francisco Massa, Daniel Haziza, Loubna Wehrstedt, Jianyuan Wang, Timothée Darcet, Théo Moutakanni, Lorena Sentana, Cameron Roberts, Andrea Vedaldi, James Tolan, Jasper Brandt, Camille Couprie, Julien Mairal, Hervé Jégou, Pierre Labatut, and Piotr Bojanowski. DINOv3. *arXiv preprint arXiv:2508.10104*, 2025. 1, 2, 3, 4, 5, 6, 8
- [42] Jianlin Su, Murtadha Ahmed, Yu Lu, Shengfeng Pan, Wen Bo, and Yunfeng Liu. RoFormer: Enhanced Transformer with Rotary Position Embedding. *Neurocomputing*, 568, 2024. 5
- [43] Ashish Vaswani, Noam Shazeer, Niki Parmar, Jakob Uszkoreit, Llion Jones, Aidan N. Gomez, Lukasz Kaiser, and Illia Polosukhin. Attention is all you need. In *NeurIPS*, 2017. 3
- [44] Huiyu Wang, Yukun Zhu, Hartwig Adam, Alan Yuille, and Liang-Chieh Chen. MaX-DeepLab: End-to-end panoptic segmentation with mask transformers. In *CVPR*, 2021. 2
- [45] Mark Weber, Jun Xie, Maxwell Collins, Yukun Zhu, Paul Voigtlaender, Hartwig Adam, Bradley Green, Andreas Geiger, Bastian Leibe, Daniel Cremers, et al. STEP: Segmenting and Tracking Every Pixel. 2021. 5
- [46] Chunlong Xia, Xinliang Wang, Feng Lv, Xin Hao, and Yifeng Shi. ViT-CoMer: Vision transformer with convolutional multi-scale feature interaction for dense predictions. In *CVPR*, 2024. 2
- [47] Linjie Yang, Yuchen Fan, and Ning Xu. Video Instance Segmentation. In *ICCV*, 2019. 5, 8
- [48] Linjie Yang, Yuchen Fan, and Ning Xu. Video instance segmentation. In *ICCV*, 2019. 3
- [49] Qihang Yu, Huiyu Wang, Siyuan Qiao, Maxwell Collins, Yukun Zhu, Hartwig Adam, Alan Yuille, and Liang-Chieh Chen. k-means mask transformer. In *ECCV*, 2022. 2, 7
- [50] Tao Zhang, Xingye Tian, Yu Wu, Shunping Ji, Xuebo Wang, Yuan Zhang, and Pengfei Wan. DVIS: Decoupled video instance segmentation framework. In *CVPR*, 2023. 3, 8
- [51] Tao Zhang, Xingye Tian, Yikang Zhou, Shunping Ji, Xuebo Wang, Xin Tao, Yuan Zhang, Pengfei Wan, Zhongyuan Wang, and Yu Wu. DVIS++: Improved Decoupled Framework for Universal Video Segmentation. *PAMI*, 2025. 3, 8
- [52] Bolei Zhou, Hang Zhao, Xavier Puig, Sanja Fidler, Adela Barriuso, and Antonio Torralba. Scene parsing through ADE20K dataset. In *CVPR*, 2017. 5, 7
- [53] Yikang Zhou, Tao Zhang, Shunping Ji, Shuicheng Yan, and Xiangtai Li. Improving video segmentation via dynamic anchor queries. In *ECCV*, 2024. 3, 8